J Polym Res (2017) 24: 200
https://doi.org/10.1007/s10965-017-1374-5

ORIGINAL PAPER

Enhancing the grafting amount of Poly(ε-caprolactone) on MgO nanoparticles by modifying with ethylene glycol for improving mechanical properties of Poly(ε-caprolactone)

Yue Lu [1,2,3] · Jianfei Cao [1,3] · Jian Huang [1,3] · Zuochun Xiong [1] · Hechun Chen [1] · Chengdong Xiong [1] · Dongliang Chen [1]

Received: 4 May 2017 / Accepted: 23 October 2017 / Published online: 31 October 2017

Abstract A new surface modification method to improve the graft polymerization of ε-caprolactone (CL) on MgO surface was developed. The MgO nanoparticles were first modified with ethylene glycol (EG), and then used for initiating graft polymerization of CL. The modified MgO nanoparticles were attested by fourier transform infrared spectroscopy, thermal gravimetric analysis and dispersion stability test. The results showed that EG was successfully grafted onto the MgO surface, the hydroxyl group of the grafted EG initiated the graft polymerization of CL onto the MgO surface in the presence of stannous octanoate. The PCL grafting amount (11.13%) on MgO modified with EG (MgO-EG) is much higher than that of unmodified MgO (3.95%). MgO-EG-PCL with 11.13 wt% of grafted PCL exhibited the most excellent dispersibility in chloroform. The MgO-EG-PCL/PCL composites exhibited the most significant improvement, tensile strength and the elongation at break of PCL increased from 15.64 to 19.58 MPa and from 272.34% to 420.73%, respectively.

Keywords Poly(ε-caprolactone) · MgO nanoparticles · Surface modification · Nanocomposite · Mechanical properties

✉ Dongliang Chen
1633cdl@cioc.ac.cn

[1] Chengdu Institute of Organic Chemistry, Chinese Academy of Sciences, Chengdu 610041, China

[2] School of Materials Science and Engineering, Sichuan University of Science and Engineering, Zigong 643000, China

[3] University of Chinese Academy of Sciences, Beijing 100049, China

Introduction

Polycaprolactone (PCL) is a semi-crystalline, hydrophobic, biocompatible, and biodegradable polymer that has extensively been used in packaging materials and biomedical applications [1–4]. However, PCL has some drawbacks including poor cell adhesion, slow biodegradation and crystallization rate, poor mechanical properties and low melting temperature (60 °C) that limited its practical application [5–7].

In the previous studies, several inorganic fillers have been added to the PCL matrix, such as clay [8, 9], carbon nanotubes [10–12], silica nanoparticles [13], titanium dioxide [14] and so on, which improved the physical properties and extend practical application of PCL. However, the impacts of these fillers on human body are unclear as biomedical material and they cannot fully biodegrade. Magnesium and its oxide are nontoxic and harmless to human body [15, 16]. Magnesia nanoparticles are selected as the inorganic filler based on the following reasons. First, magnesia nanoparticles are alkaline oxide, which can act as a buffer to reduce the inflammatory reaction by neutralizing the acidic by-product of PCL degradation. Second, magnesium is an essential element of human body and magnesium ion is nontoxic [17].

For polymer/MgO composites, the interaction and adhesion between the MgO filler and the polymer matrix is a critical factor to determine the mechanical properties of the composite because the lack of adhesion between the two phases will result in an early failure at the interface, thus deteriorating the mechanical properties [18]. To solve this situation, it is necessary to increase the compatibility between the filler and the polymer. Various methods have been developed to improve adhesion between MgO and a particular polymeric matrix, for example, silane coupling agents [19], stearic acid [20], aluminum acid ester [21] and oligo-L-lactide [22, 23]. These molecules were grafted on the surface of MgO particles

through covalent bonds by the chemical reaction with the hydroxyl groups on the surface of MgO particles. However, because the number of active hydroxyl groups on the MgO particles is limited and the reactivity of these hydroxyl groups is reasonably low, only a little amount of grafted organic molecules was obtained in these researches.

To the best of our knowledge, there are few reports about the utilization of MgO and PCL-grafted-MgO nanoparticles for the reinforcement of PCL, and no systemic study has yet been dedicated to considering the effects of the reactivity of hydroxyl groups on the MgO nanoparticles, which will influence the grafting amount of PCL and the mechanical properties of MgO/PCL nanocomposites.

In this paper, a new approach to improve the reactivity of hydroxyl groups on the MgO and the adhesion between MgO and the PCL matrix was reported. The MgO nanoparticles were first reacted with hexamethylene diisocyanate (HMDI) and further with EG, and at last used for initiating graft polymerization of CL. In this way, the reactivity of hydroxyl groups on the MgO nanoparticles would be improved and the grafting amount of MgO for PCL would be greatly enhanced. The connection between MgO and PCL would be also strengthened, improving the interaction and adhesion of MgO nanoparticles in the composite. Hence, the excellent mechanical properties would be obtained.

Experiments

Materials

Magnesium oxide (MgO) powder with average diameter of 50 nm and purity of 99.9% was provided by Macklin Biochemical Co.,Ltd. (Shanghai, China). PCL (molecular weight (Mw) of the 166 kg/mol), was purchased from Chengdu Organic Chemicals Co.,Ltd. (Chengdu, China). CL was purchased from Sigma(USA), dried over calcium hydride and vacuum distilled. Stannous octoate was purchased from Sigma (USA). N,N-Dimethylformamide(DMF) was vacuum distilled over anhydrous magnesium sulfate. Prior to use, Toluene was distilled from calcium hydride under N_2. prior to use. All other agents used were of analytical grade and did not require further treatment.

Surface modification of MgO with EG

To a stirred suspension of MgO (4 g) in dry DMF (50 mL) were added HMDI (2 mL,) and dibutyltindilaurate (0.1 ml). The reaction was maintained at 70 °C under nitrogen for 12 h. A solution of EG (7 mL) in DMF (10 mL) was added to the reaction mixture, and the mixture was stirred for 12 h. After the reaction, EG-grafted MgO (MgO-EG) was purified and collected by repeated washing with methylene chloride and centrifugation at 2000 rpm for 10 min (5 cycles). The isolated MgO-EG was dried at 40 °C in vacuo for 48 h.

Graft polymerization of CL on MgO and MgO-EG nano-particles

MgO (3 g) was dried at 120 °C under vacuum for 24 h and transferred to a flask containing CL (6 g) and $Sn(oct)_2$ (0.06 g in 50 mL dry toluene), and stirred to suspension under a neat dry nitrogen purge. The flask was heated up to 130 °C and this temperature was maintained for 24 h. The mixture was cooled down to room temperature and diluted with methylene chloride. The MgO-PCL powder was separated by a repeated washing-centrifugation (5 cycles) at 2000 rpm for 10 min to remove the potentially unreacted ε-caprolactone and the free PCL homo-polymer chains formed during the reaction. Finally, the MgO-PCL particles were dried in a vacuum oven at room temperature for 48 h. Another PCL-grafted MgO (MgO-EG-PCL), which were obtained using MgO-EG, were synthesized under the same conditions as MgO-PCL.

Preparation of PCL composite films

MgO, MgO-PCL, and MgO-EG-PCL were dispersed separately in chloroform, and PCL was added to each suspension to prepare the solution mixture. Each solution was poured into an excess of ethanol to precipitate the PCL/MgO, PCL/MgO-PCL, and PCL/MgO-EG-PCL nanocomposites, respectively. The composites were dried in vacuo at room temperature for 48 h.

The PCL only, PCL/MgO, PCL/MgO-PCL and PCL/MgO-EG-PCL composites underwent the thermally melting and hot-pressing process using compression press XLB-350.350.2 (Jinma Golden Horse Co.,Ltd., Haimen, China). 1.2 g of polymer mixture was put on the hot-press plate, and the plate temperature was then raised to 100 °C. After melting time of 5 min, the pressure increased to about 10 MPa and maintained for press time of 5 min. The dimension of compressively molded specimens was 50 × 30 mm^2 and its thickness was 0.5 mm.

Fourier transform infrared (FT-IR) spectroscopy

FTIR spectra were recorded on an FT-IR 6700 spectrometer (Thermo Nicolet, USA) in the range between 4000 and 400 cm^{-1}. All the samples were mixed with KBr powder and pressed into discs prior to spectra acquisition.

Thermal gravimetric analysis (TGA)

About 3–5 mg of samples was placed in a platinum sample pan of a TGA Q500 (TA, USA). The testing temperature ranged from room temperature to 600 °C. The testing was performed under a nitrogenous atmosphere at a heating rate of 10 °C/min.

Dipersion stability test

Dispersion stability of different MgO nano-particles was evaluated in chloroform by a sedimentation experiment and a dynamic light scattering (DLS) analysis. 1 wt.% of MgO nanoparticles were added in 50 ml chloroform. The nanoparticles were then dispersed by ultrasonic irradiating for 30 min and stirred for further 2 h. The suspensions further subjected to 10 min ultrasonic irradiation and were allowed to stand for at least 5 h. The particles sedimentation behavior was observed.

The particle size, size distributions and zeta potential of different MgO nano-particles were tested using a DLS system (Mastersizer 2000, Malvern Instruments Ltd., UK).

Mechanical properties

The mechanical properties such as tensile strength and elongation were measured by a universal testing machine CMT4503 (Sans Testing Machine Co.,Ltd.,Shenzhen, China). The rectangular tensile specimens with a dimension of 50 mm × 5 mm × 0.5 mm were cut from the films. The cross-head speed was 50 mm/min. Every specimen would be parallel determined five times. The averages were calculated based on the five raw data.

Scanning electron microscopy (SEM)

Morphologies of quenching fracture surfaces of composite films were observed by field emission scanning electron microscope Inspect F50 (FEI, USA). A layer of gold was sprayed over the surface before observation.

Results and discussions

Grafting of CL on the surface of different MgO nano-particles

The PCL was grafted on the surface of MgO nano-particles through the ring opening polymerization of CL monomers. Under the catalysis of stannous octoate ($Sn(Oct)_2$), the reaction was initiated by the hydroxyl groups available on the surface of the MgO nano-particles. For the study of graft polymerization, the grafting reaction was performed using two different methods as shown in Fig. 1. In reaction a, the surface hydroxyl groups on MgO nano-particles were directly used for initiating graft polymerization of CL. For reaction b, surface hydroxyl groups were first reacted with HMDI and further with EG, and at last used for initiating graft polymerization of CL. The modified MgO in each reaction was denoted as MgO-PCL, MgO-HDMI, MgO-EG, and MgO-EG-PCL, respectively. We started the grafting reaction on the assumption that the different chemical reactivity of surface hydroxyl groups may determine the efficiency of graft polymerization of CL on MgO nanoparticles.

FTIR spectroscopy analysis

Figure 2 showed FTIR spectra of unmodified MgO, MgO-HDMI, MgO-EG, PCL, MgO-PCL and MgO-EG-PCL nanoparticles. As shown in Fig. 2a, the spectra of MgO were typical [21, 22]. The absorption peak at 1431 cm^{-1} of MgO was ascribed to the characteristic vibration of Mg-O bond. The broad absorption peak at 3446 cm^{-1} was assigned to the interactions between hydroxyl groups (−OH) on the surfaces of the MgO nano-particles. The layer of –OH from water dissociation would cover the outmost surfaces of many inorganic particles [24, 25]. The IR spectrum of MgO-HDMI in Fig. 2b obviously exhibited the presence of –NHCO- at 1621 and 1578 cm^{-1} and free isocyanate bands at 2270 cm^{-1}. This indicated that the isocyanate group at the one end of HMDI was coupled to MgO surfaces via chemical bonding, and the isocyanate group at the other end was still active for the reaction with EG. After reaction of MgO-HMDI with EG, isocyanate bands completely disappeared as shown in Fig. 2c, revealing the introduction of EG on MgO nanosurfaces. Compared with the spectra of pure PCL(Fig. 2d),the C = O stretching at 1733 cm^{-1} was observed for MgO-PCL(Fig. 2e) and MgO-EG-PCL(Fig. 2f) nanoparticles, which suggested that PCL chains were grafted onto the surfaces of MgO and MgO-EG nanoparticles.

TGA analysis

Figure 3 showed TGA curves of unmodified MgO, MgO-PCL, MgO-EG and MgO-EG-PCL nano-particles. The weight losses of unmodified MgO, MgO-PCL, MgO-EG and MgO-EG-PCL were 4.92%, 8.87%, 9.39% and 20.52%, respectively. The amounts of surface-grafted PCL on MgO and MgO-EG were calculated as follows:

$$M_{PCL}(\mathrm{MgO}) = W(\mathrm{MgO\text{-}PCL}) - W(\mathrm{MgO}) = 8.87\,\% - 4.92\,\% = 3.95\,\%$$
$$M_{PCL}(\mathrm{MgO\text{-}EG}) = W(\mathrm{MgO\text{-}EG\text{-}PCL}) - W(\mathrm{MgO\text{-}EG}) = 20.52 - 9.39\% = 11.13\%$$

As listed above,the PCL grafting amount on MgO-EG (11.13%) is much higher than that of MgO (3.95%). There are two possible reasons to explain this enhanced grafting efficiency of MgO-EG for PCL: One is the nucelophilicity

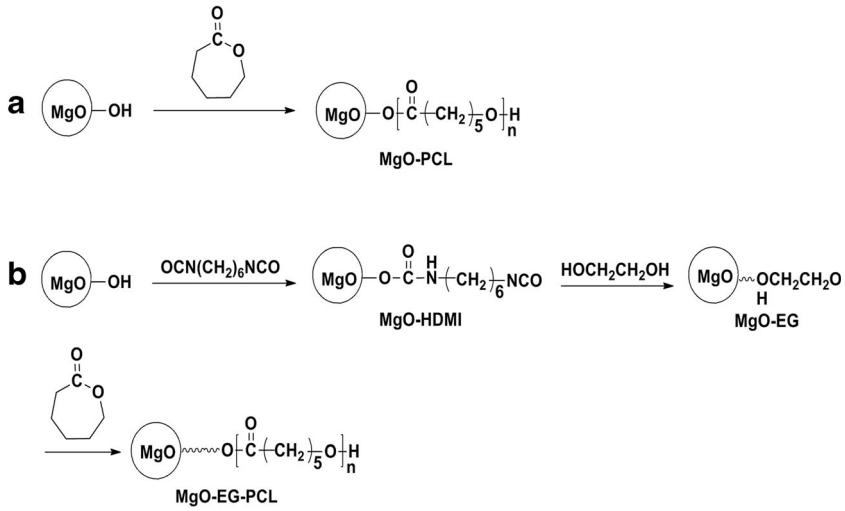

Fig. 1 Reaction routes for grafting reaction of CL on MgO nanosurfaces

of hydroxyl groups on MgO surfaces. The hydroxyl groups on MgO-EG are primary -OH, and thus they can initiate the polymerization of CL more easily than surface hydroxyl groups on unmodified MgO. The other is the steric environment of hydroxyl groups. The hydroxyl groups of MgO-EG are linked to the MgO surface via a relatively long chain spacer. For this reason, the steric hindrance of the hydroxyl group seems to be very low, and it may have more accessibility to CL for graft polymerization [26]. Thus, it can be suggested that the key factor for effective graft polymerization of CL is ascribed to reactivity of the surface hydroxyl groups.

Dispersion stability test in chloroform

The dispersity of different MgO nano-particles in chloroform was tested by a sedimentation experiment and a DLS analysis. The sedimentation behavior of three types MgO nanoparticles are shown in Fig. 4. As Xu et al. reported [27], two types of sedimentation mechanisms could be observed: flocculation and accumulation. For sample containing unmodified MgO, the sedimentation was mainly driven by flocculation. The suspension separated very quickly into sediments (within 3 min) and clear supernatant on top of the sediment was observed. The separation interfaces

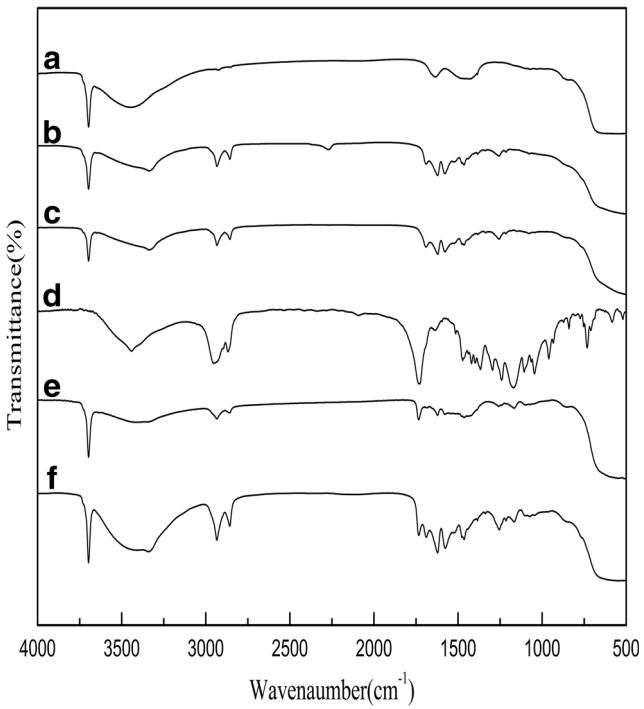

Fig. 2 FTIR spectra of (**a**) unmodified MgO, (**b**) MgO-HDMI, (**c**) MgO-EG, (**d**) PCL, (**e**) MgO-PCL and (**f**) MgO-EG-PCL

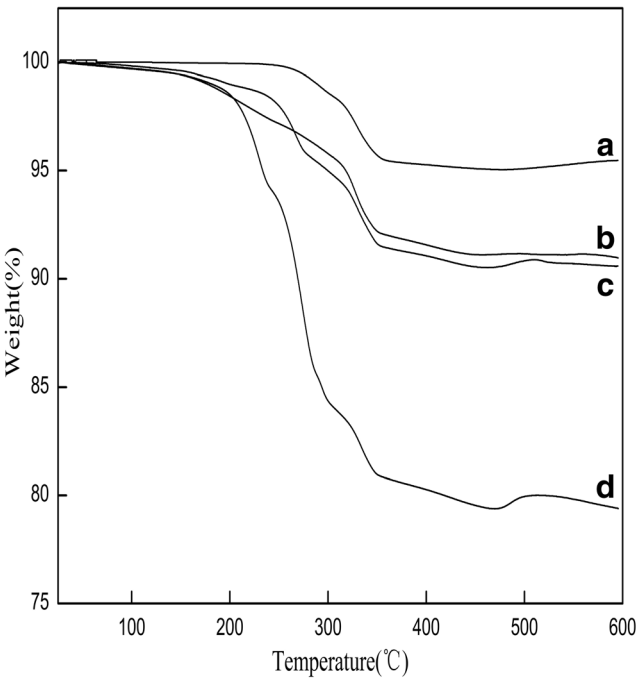

Fig. 3 TGA thermograms of (**a**) unmodified MgO, (**b**) MgO-PCL, (**c**) MgO-EG and (**d**) MgO-EG-PCL

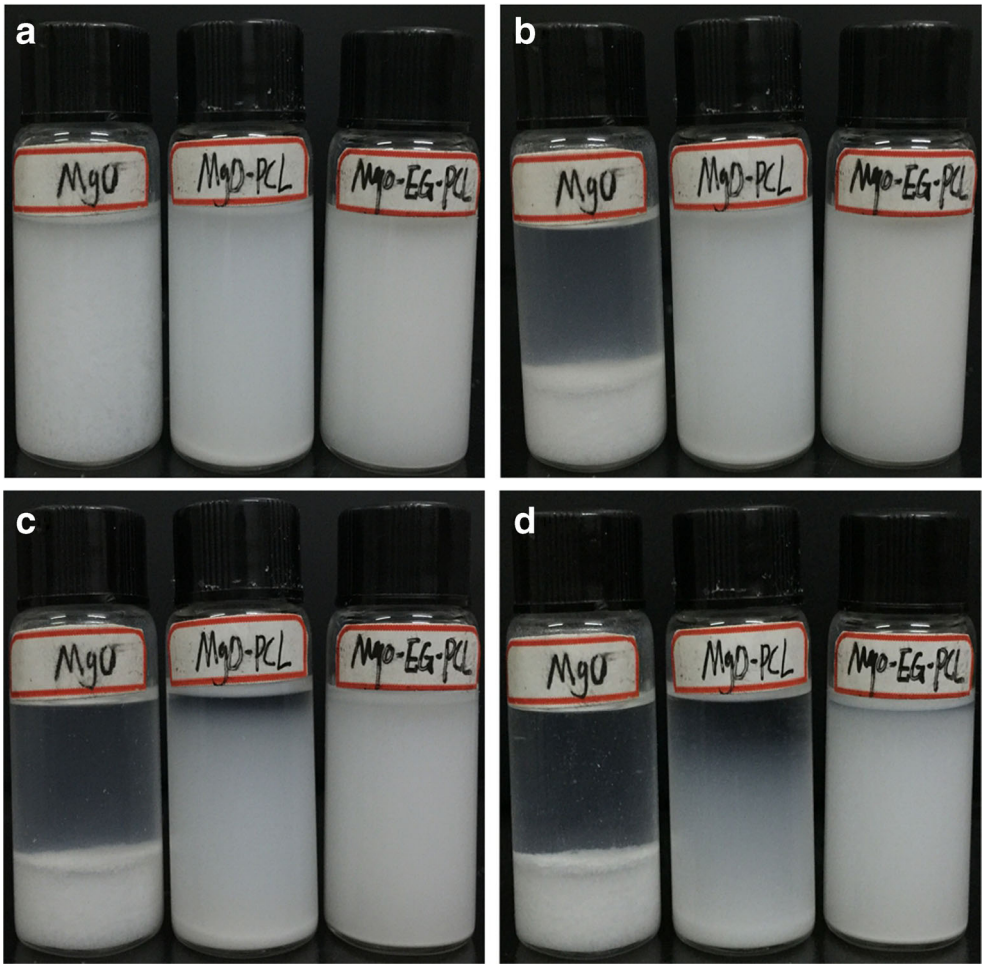

Fig. 4 Sedimentation behavior of unmodified MgO, MgO-PCL and MgO-EG-PCL in chloroform: (**a**) 0 min, (**b**) 3 min, (**c**) 1 h, (**d**) 5 h

between the sediment and the supernatant were sharp and moved downward with time. For samples containing MgO-PCL, the nanoparticles settled slowly into sediments and partly clear supernatant on top of the suspensions was observed within 5 h. Solution contaning MgO-EG-PCL exhibited the most turbidity. This sedimentation behavior was typical of well-dispersed suspensions and the particles had much slower settling rates, which might be counter balanced by Brownian motion, they remained in the supernatant for long time. Even after 5 h the solution containing MgO-EG-PCL remained turbid.

DLS technique was used to analyze the size, size distributions and zeta potential of MgO nanonparticles. As we know, nanonparticles tend to aggregate due to the strong interaction, therefore the size of nanonparticles in the solvent can reflect the dispersion state in solution. As shown in Fig. 5, the average particle size of MgO in chloroform was about 3200 nm, while the average particle size of MgO-PCL and MgO-EG-PCL changed into 502 nm and 103 nm, and showed narrower distribution in comparison with MgO. The magnitude of the zeta potential indicates the degree of electrostatic repulsion or attraction between particles in dispersion. Zeta potential measurements showed that the zeta potentials of MgO, MgO-PCL and MgO-EG-PCL were 6.2 mV, 17.8 mV and 25.9 mV, respectively.

These above results suggested that the MgO-PCL nanoparticles showed a much improved dispersion property, compared with unmodified MgO. Besides, the dispersion state was further improved due to the increased grafting amount of PCL. MgO-EG-PCL with 11.13 wt% of grafted PCL exhibited the most excellent dispersibility in chloroform.

Mechanical properties of the nanocomposites

As mentioned above, the grafting amount of PCL on MgO greatly enhanced the dispersion property, the next question is whether the PCL-grafted MgO in the MgO/PCL nanocomposites can play a important role in improving the mechanical properties of the composites. Figure 6 showed the stress-strain profile of neat PCL, MgO/PCL, MgO-PCL/PCL, and MgO-EG-PCL/PCL, respectively. The values of tensile strength and elongation at break derived from the

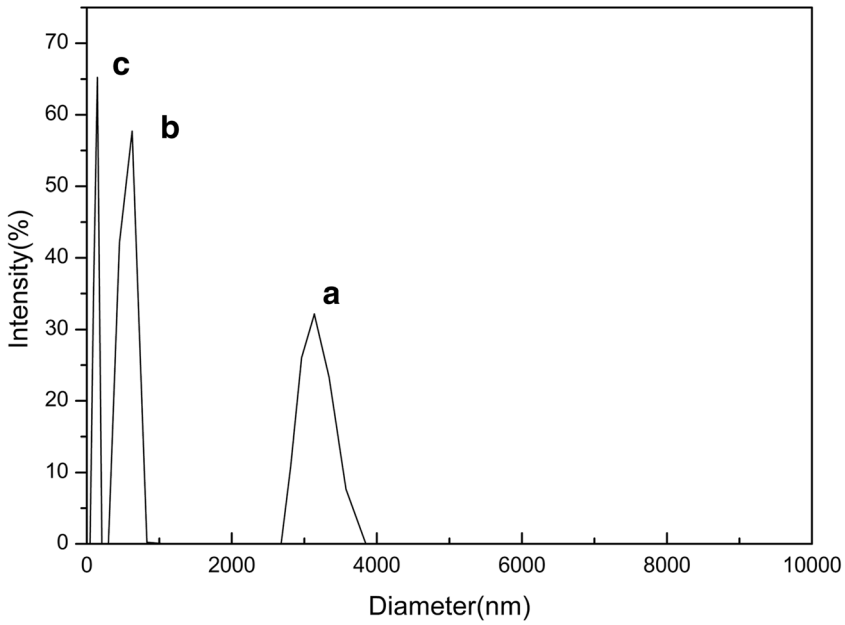

Fig. 5 Size and size distribution (in diameter, nm) detected by DLS technique of (**a**) unmodified MgO, (**b**) MgO-PCL and (**c**) MgO-EG-PCL in chloroform (1 mg/mL)

curves are summarized in Table 1. Neat PCL underwent the typical stress-stain behavior of semicrystalline elastic polymers, yielding, rubbery plateau, and fracture. The nanocomposites exhibited the similar behavior. For the MgO/PCL composite, the addition of MgO (6 wt%) into the PCL matrix increased the tensile strength from 15.64 to 16.36 MPa, but decreased the elongation at break from 272.34% to 212.68%. The MgO-PCL/PCL composites showed higher tensile strength and the elongation at break. The MgO-EG-PCL/PCL composites exhibited the most significant improvement, tensile strength and the elongation at break of PCL increased by 25.2% and 54.5%, respectively. This may be ascribed to the dispersion state and interfacial adhesion between the different MgO nanoparticles and the PCL matrix, which needs to be investigated with further FE-SEM characterization.

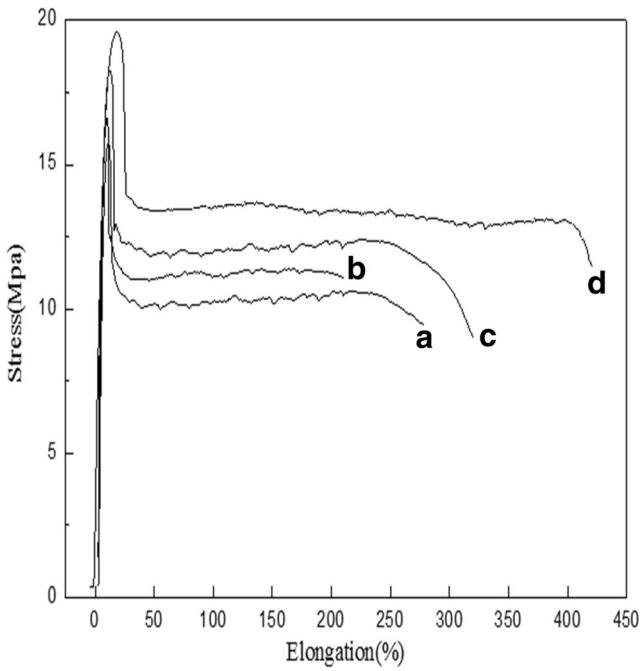

Fig. 6 Typical stress-strain diagram of (**a**) neat PCL, (**b**) MgO/PCL 6 wt%, (**c**) MgO-PCL/PCL 6 wt%, and (**d**) MgO-EG-PCL/PCL 6 wt%

FE-SEM observation of the nanocomposites

The quenching fracture surfaces of the neat PCL, MgO/PCL, MgO-PCL/PCL and MgO-EG-PCL/PCL composites were observed by FE-SEM (Fig. 7). From the micrographs, the modified MgO particles (MgO-PCL, MgO-EG-PCL; Fig. 7c,d) could disperse more uniformly in the PCL matrix than pure MgO (Fig. 7b). More agglomerated and aggregated particles of diameter 10 μm could be found in MgO/PCL composites. In addition, it can be seen that there was a serious phase separation phenomenon between the MgO and PCL matrix, and this incompatibility situation was improved in MgO-PCL/PCL composites. However, the MgO-EG-PCL nanoparticles were embedded in and entangled tightly with the matrix, and hardly any phase separation can be observed. The results may be explained that the grafted PCL chains on the surfaces of MgO-EG-PCL, as inter-tying molecules, played an important role in forming the molecule chains entanglement and improving the interfacial adhesion between the MgO-EG-PCL and PCL matrix. The strong interfacial adhesion can result in efficient stress transfer from PCL matrix to the MgO-EG-PCL nanoparticles, which can increase the ability of the material to absorb energy and improve the mechanical properties of composite.

Table 1 Mechanical Properties of neat PCL, MgO/PCL, MgO-PCL/PCL and MgO-EG-PCL/PCL

Sample	Tensile strength (MPa)	Elongation at break (%)
neat PCL	15.64	272.34
MgO/ PCL (6 wt%)	16.36	212.68
MgO-PCL/PCL (6 wt%)	18.28	323.62
MgO-EG-PCL/PCL (6 wt%)	19.58	420.73

Conclusion

In this work, EG was successfully grafted onto the MgO surface, the hydroxyl group of the grafted EG initiated the graft polymerization of CL onto the MgO surface in the presence of stannous octanoate. In this way, the reactivity of hydroxyl groups and the PCL grafting amount on the MgO surface were greatly enhanced, as compared with unmodified MgO. Due to the uniform dispersion and strong interfacial adhesion between MgO-EG-PCL and the PCL matrix, the mechanical properties of PCL were significantly improved, tensile strength and the elongation at break of PCL increased by 25.2% and 54.5%, respectively.

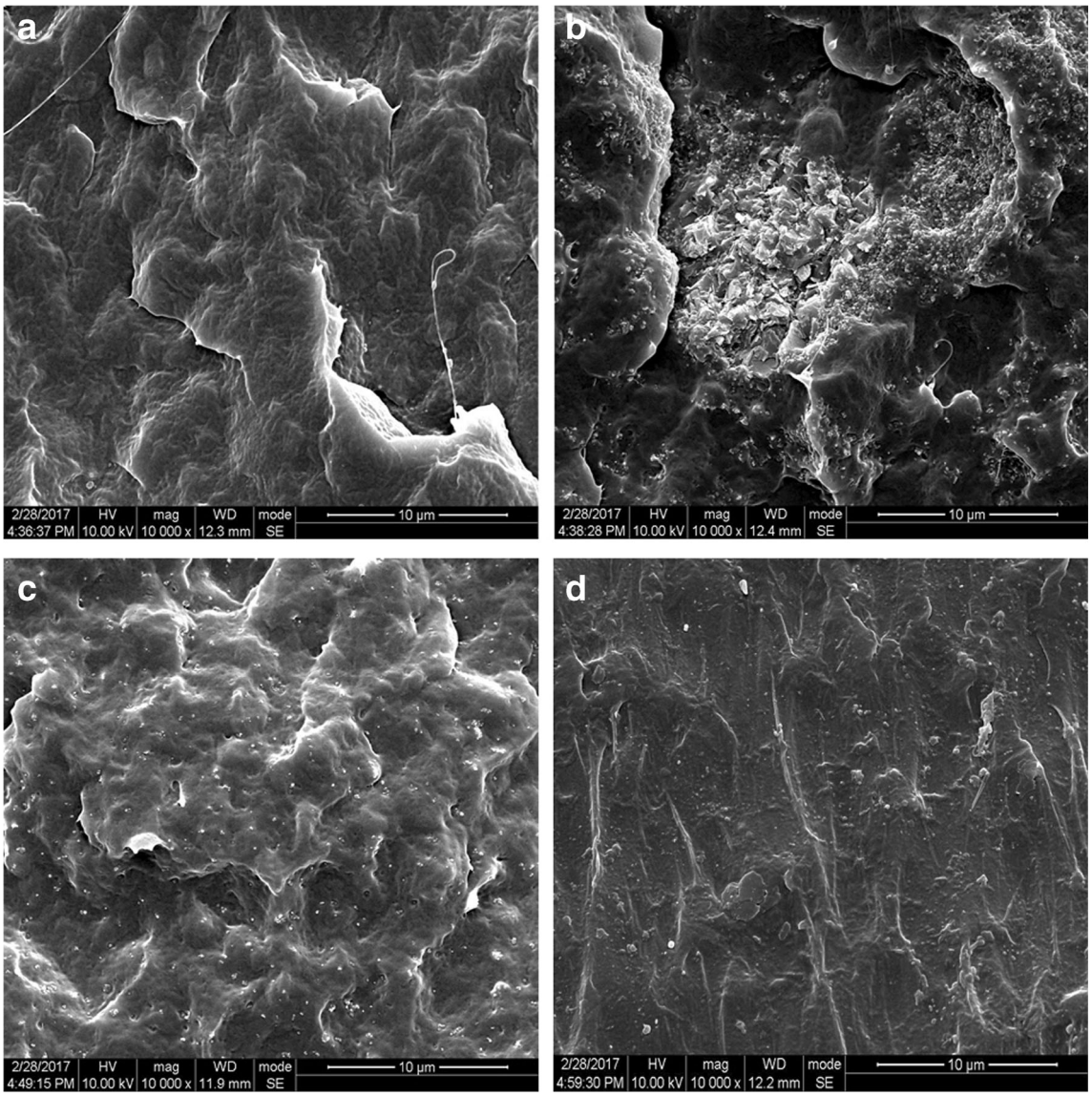

Fig. 7 FE-SEM micrographs of the quenching fracture surfaces of (**a**) neat PCL, (**b**) PCL/MgO, (**c**) PCL/MgO-PCL and (**d**) PCL/MgO-EG-PCL composites

Acknowledgements This research was supported by the Science and Technology supporting program of Sichuan province, China (No.2014SZ0128).

References

1. Woodruff MA, Hutmacher DW (2010) The return of a forgotten polymer-Polycaprolactone in the 21st century. Prog Polym Sci 35: 1217–1256
2. Labet M, Thielemans W (2009) Synthesis of polycaprolactone: a review. Chem Soc Rev 38:3484–3504
3. Kweon H, Yoo MK, Park IK, Kim TH, Lee HC, Lee HS, JS O, Akaike T, Cho CS (2003) A novel degradable polycaprolactone networks for tissue engineering. Biomaterials 24:801–808
4. Augustine R, Malik HN, Singhal DK, Mukherjee A, Malakar D, Kalarikkal N, Thomas S (2014) Electrospun polycaprolactone/ZnO nanocomposite membranes as biomaterials with antibacterial and cell adhesion properties. J Polym Res 21:347
5. Wang Y, Yang J-F (2010) Physical properties and biodegradation of acrylic acid grafted poly(epsilon-caprolactone)/chitosan blends. J Polym Res 17:221–232
6. Mofokeng JP, Luyt AS (2015) Morphology and thermal degradation studies of melt-mixed poly(hydroxybutyrate-co-valerate) (PHBV)/poly(epsilon-caprolactone) (PCL) biodegradable polymer blend nanocomposites with TiO2 as filler. J Mater Sci 50:3812–3824
7. Mallakpour S, Nouruzi N (2016) Modification of morphological, mechanical, optical and thermal properties in polycaprolactone-based nanocomposites by the incorporation of diacid-modified ZnO nanoparticles. J Mater Sci 51:6400–6410
8. Jimenez G, Ogata N, Kawai H, Ogihara T (1997) Structure and thermal/mechanical properties of poly(epsilon-caprolactone)-clay blend. J Appl Polym Sci 64:2211–2220
9. Luduena LN, Kenny JM, Vazquez A, Alvarez VA (2014) Effect of extrusion conditions and post-extrusion techniques on the morphology and thermal/mechanical properties of polycaprolactone/clay nanocomposites. J Compos Mater 48:2059–2070
10. Chen E-C, T-M W (2007) Isothermal crystallization kinetics and thermal behavior of poly(epsilon-caprolactone)/multi-walled carbon nanotube composites. Polym Degrad Stab 92:1009–1015
11. Yeh J-T, Yang M-C, C-J W, C-S W (2009) Preparation and characterization of biodegradable Polycaprolactone/multiwalled carbon nanotubes nanocomposites. J Appl Polym Sci 112:660–668
12. Pan L, Pei X, He R, Wan Q, Wang J (2012) Multiwall carbon nanotubes/polycaprolactone composites for bone tissue engineering application. Colloid Surface B 93:226–234
13. Catauro M, Raucci MG, De Gaetano F, Marotta A (2003) Sol-gel synthesis, characterization and bioactivity of polycaprolactone/SiO2 hybrid material. J Mater Sci 38:3097–3102
14. Gupta KK, Kundan A, Mishra PK, Srivastava P, Mohanty S, Singh NK, Mishra A, Maiti P (2012) Polycaprolactone composites with TiO2 for potential nanobiomaterials: tunable properties using different phases. Phys Chem Chem Phys 14:12844–12853
15. Staiger MP, Pietak AM, Huadmai J, Dias G (2006) Magnesium and its alloys as orthopedic biomaterials: a review. Biomaterials 27: 1728–1734
16. Song G (2007) Control of biodegradation of biocompatable magnesium alloys. Corros Sci 49:1696–1701
17. Jia J, Yang J, Zhao Y, Liang H, Chen M (2016) The crystallization behaviors and mechanical properties of poly(L-lactic acid)/magnesium oxide nanoparticle composites. RSC Adv 6:43855–43863
18. Qiu XY, Hong ZK, JL H, Chen L, Chen XS, Jing XB (2005) Hydroxyapatite surface modified by L-lactic acid and its subsequent grafting polymerization of L-lactide. Biomacromolecules 6: 1193–1199
19. Chen S-s HJ, Gao L, Zhou Y, S-m P, He J-l, Z-m D (2016) Enhanced breakdown strength and energy density in PVDF nanocomposites with functionalized MgO nanoparticles. RSC Adv 6: 33599–33605
20. Zhao Y, Liu B, You C, Chen M (2016) Effects of MgO whiskers on mechanical properties and crystallization behavior of PLLA/MgO composites. Mater Design 89:573–581
21. Zhao Y, Liu B, Yang J, Jia J, You C, Chen M (2016) Effects of modifying agents on surface modifications of magnesium oxide whiskers. Appl Surf Sci 388:370–375
22. Wen W, Luo B, Qin X, Li C, Liu M, Ding S, Zhou C (2015) Strengthening and toughening of poly(L-lactide) composites by surface modified MgO whiskers. Appl Surf Sci 332:215–223
23. Zou Z, Luo C, Luo B, Wen W, Liu M, Zhou C (2016) Synergistic reinforcing and toughening of poly(L-lactide) composites with surface-modified MgO and chitin whiskers. Compos Sci Technol 133:128–135
24. Al-Abadleh HA, Grassian VH (2003) Oxide surfaces as environmental interfaces. Surf Sci Rep 52:63–161
25. Al-Abadleh HA, Al-Hosney HA, Grassian VH (2005) Oxide and carbonate surfaces as environmental interfaces: the importance of water in surface composition and surface reactivity. J Mol Catal A-Chem 228:47–54
26. Lee HJ, Choi HW, Kim KJ, Lee SC (2006) Modification of hydroxyapatite nanosurfaces for enhanced colloidal stability and improved interfacial adhesion in nanocomposites. Chem Mater 18: 5111–5118
27. Xu X, Oliveira M, Ferreira JMF (2003) Effect of solvent composition on dispersing ability of reaction sialon suspensions. J Colloid Interface Sci 259:391–397